NASA TECHNICAL NOTE

NASA TN D-5024

WIND-TUNNEL STUDY OF DEFLECTED-ELEVATOR FLUTTER ENCOUNTERED ON A T-TAIL AIRPLANE

by Maynard C. Sandford and Charles L. Ruhlin

Langley Research Center
Langley Station, Hampton, Va.

NATIONAL AERONAUTICS AND SPACE ADMINISTRATION • WASHINGTON, D. C. • FEBRUARY 1969

WIND-TUNNEL STUDY OF DEFLECTED-ELEVATOR FLUTTER ENCOUNTERED ON A T-TAIL AIRPLANE

By Maynard C. Sandford and Charles L. Ruhlin

Langley Research Center
Langley Station, Hampton, Va.

NATIONAL AERONAUTICS AND SPACE ADMINISTRATION

For sale by the Clearinghouse for Federal Scientific and Technical Information
Springfield, Virginia 22151 – CFSTI price $3.00

WIND-TUNNEL STUDY OF DEFLECTED-ELEVATOR FLUTTER ENCOUNTERED ON A T-TAIL AIRPLANE

By Maynard C. Sandford and Charles L. Ruhlin
Langley Research Center

SUMMARY

An exploratory study of a horizontal-tail flutter encountered on the T-tail of a large multijet cargo airplane has been conducted in the Langley transonic dynamics tunnel at Mach numbers up to 0.93. The airplane flutter, consisting primarily of a coupled elevator-rotation and stabilizer-torsion oscillation at about 24 cps, occurred at a Mach number near 0.8 at several altitudes and was initiated only when the elevators were deflected about 8° or greater. The wind-tunnel study employed a 1/8.5-size flutter model which consisted of a geometrically, dynamically, and elastically scaled empennage and aft fuselage, and dynamically and elastically, but not geometrically, simulated wings, nacelles, and forward fuselage.

The basic flutter phenomenon experienced on the airplane was reproduced by the model in the wind tunnel although the model predicted considerably higher flutter speeds than those of the airplane at Mach number 0.8. The model flutter speed boundary was nearly flat from a Mach number of 0.41 to 0.89 and rose sharply and curved inward tending to form a closed flutter region at the extreme Mach numbers. In order to initiate model flutter, an elevator deflection angle of 8° in the trailing-edge-down attitude was required, whereas on the airplane, flutter occurred for an elevator deflection of 8° in either an up or down direction. Changing stabilizer pitch angle within a limited range reduced the flutter amplitude but never completely suppressed the flutter. Elevator mass balancing, used to eliminate flutter on the airplane, also eliminated flutter on the model.

INTRODUCTION

During high-altitude flight tests of a large multijet cargo airplane having a T-tail, an unstable oscillation of the horizontal tail was encountered at Mach numbers near 0.8 (ref. 1). This instability, consisting primarily of a coupled elevator-rotation and stabilizer-torsion oscillation at about 24 cycles per second, was initiated during flight maneuvers requiring gradual deflection of the elevators when the elevators reached angles of about $\pm 8^{\circ}$ relative to the stabilizer chord plane. Elevator deflections of this magnitude or greater were in all instances a necessary condition for the instability. Several fixes

commonly used for alleviating control surface instabilities at high Mach numbers were investigated on subsequent flight tests, but none appreciably affected the instability. These fixes included vortex generators on the stabilizer, aerodynamic wedges and small viscous dampers on the elevators, and small increases in elevator mass balance. A simplified flutter analysis employing two degrees of freedom (uncoupled elevator-rotation and stabilizer-torsion modes) and incompressible flow coefficients was made (ref. 1), and by modifying the elevator aerodynamic hinge-moment derivative, an airplane flutter condition was obtained. This modified analysis indicated that the flutter speed could be raised significantly by large increases either in the elevator mass balance or in elevator damping. Since elevator mass balancing appeared to be a practical and promising solution, it was tried as a fix for the airplane instability. This fix was verified by flight tests and later incorporated on these airplanes.

Although many types of dynamic instabilities involving control surfaces are described in the literature (for example, refs. 2 and 3), there is little or no information available at the present time on instabilities initiated by deflected control surfaces, especially on T-tail configurations. Therefore, the present experimental study was undertaken to determine if the instability experienced on the T-tail airplane mentioned previously could be duplicated in a wind tunnel and, if so, to explore some basic characteristics of the phenomenon. The study employed a modified model available from previous flutter investigations of this T-tail (refs. 4 and 5). The investigation was conducted at Mach numbers up to 0.93 in the Langley transonic dynamics tunnel with freon as the test medium, and included as test variables a range of elevator deflection and stabilizer incidence angles. Presented herein are the results of the experimental study.

SYMBOLS

b	stabilizer semichord at plane of symmetry, feet (meters)
EI	bending stiffness, pound-inches^2 (kilonewton-meters^2)
f	flutter frequency, cycles per second
f_e	natural frequency of elevator rotation, cycles per second
f_i	natural frequency of ith structural vibration mode, cycles per second
GJ	torsional stiffness, pound-inches^2 (kilonewton-meters^2)
I_{ea}	mass moment of inertia of stabilizer section about its elastic axis, slug-feet^2 (kilogram-meters^2)

$I_{h\ell}$ mass moment of inertia of elevator about its hinge line, slug-feet^2 (kilogram-meters^2)

I_θ mass moment of inertia in pitch about horizontal-tail pivot axis, slug-feet^2 (kilogram-meters^2)

I_ψ mass moment of inertia in yaw about a vertical axis through intersection of fin elastic axis and stabilizer horizontal plane, slug-feet^2 (kilogram-meters^2)

I_ϕ mass moment of inertia in roll about intersection of stabilizer horizontal plane and plane of symmetry, slug-feet^2 (kilogram-meters^2)

M Mach number

m_h total semispan mass of exposed horizontal-tail sections 1 to 6 and elevator, slugs (kilograms) (see table I)

q dynamic pressure, pounds per foot^2 (kilonewtons per meter^2)

R Reynolds number based on mean aerodynamic chord of horizontal tail (see fig. 2)

S_{ea} mass unbalance of stabilizer section about its elastic axis, slug-feet (kilogram-meters)

$S_{h\ell}$ mass unbalance of elevator about its hinge line, slug-feet (kilogram-meters)

V free-stream velocity, feet per second (meters per second)

V_{KEAS} equivalent airspeed, knots

v volume of a conical frustum having exposed horizontal-tail root chord as base diameter, horizontal-tail tip chord as upper diameter, and exposed horizontal-tail semispan as height; model value is 2.84 feet^3 (0.0804 meter^3)

α_s free-stream angle of attack of horizontal stabilizer, δ_s + Fuselage angle of attack, degrees

δ_e deflection angle of elevator relative to horizontal-stabilizer chord plane, positive trailing edge down, degrees

δ_s incidence angle of horizontal stabilizer relative to fuselage reference line, positive leading edge up, degrees

η_{ea} distance along elastic axis (spar center line) of stabilizer measured from plane of symmetry, fraction of elastic-axis length

η_{hl} distance along hinge line of elevators measured from control surface root, fraction of hinge-line length

μ mass ratio of horizontal tail, $m_h/\rho v$

ρ test-medium density, slugs per foot^3 (kilogram per meter^3)

Abbreviations:

BL buttock line, inches (centimeters)

FS fuselage station, inches (centimeters)

WL water line, inches (centimeters)

MODEL

General Description

The present investigation employed a model used in earlier flutter investigations (refs. 4 and 5) of the T-tail of the large multijet cargo airplane which experienced the elevator flutter during flight. Two airplane configurations were simulated on the model: the flutter configuration having the original elevator balance weights and the stable configuration with the additional elevator balance weights. A photograph of the model mounted in the tunnel and sketches of the horizontal tail are presented in figures 1 and 2. Some model properties are given in table I and figures 2 to 4.

For the purposes of the present study, primary emphasis was directed toward scaling the horizontal-tail components and the remainder of the model was considered as simply a reasonably scaled test vehicle for this surface. The horizontal-tail model used was that of an early design (ref. 5) which was similar to the current airplane planform but of slightly larger overall dimensions; therefore, a slight adjustment in length scale factor from the original value of 1/9 to 1/8.465 was required. The model was modified to scale

current airplane properties, particularly the elevator and exposed stabilizer. Some scaling factors for the horizontal-tail model are given in the appendix. The bullet fairing was also recontoured to conform to the current airplane shape.

The rest of the model consisted of the same basic components of the design version model of reference 4. The vertical tail and aft fuselage were 1/9 size, geometrically, dynamically, and elastically scaled, whereas the wings, nacelles, and forward fuselage were dynamically and elastically, but not geometrically, simulated. These components were used with only minor modifications such as shifting ballast weights in the wings and forward fuselage for trim.

Construction

The model was built by using a spar-and-pod construction technique. A single box spar provided the required stiffnesses and lightweight wooden pods gave the required shape. Gaps between the pods were aerodynamically sealed with sponge rubber. Further construction details may be found in reference 4.

The incidence angle of the horizontal stabilizer could be varied in pitch through angles of about $\pm 5^{\circ}$. Left and right elevators were flexibly interconnected to simulate roughly the carry-through stiffnesses, and elevator-rotation springs (part of the carry-through structure) were sized to give best agreement in the structural vibration frequencies. A remotely controlled mechanism was installed for rotating the elevators symmetrically through an angular range of about $\pm 15^{\circ}$ relative to the stabilizer-chord plane. The elevators were rotated (fig. 2) by a jackscrew driven through an articulated shaft by an electric motor located in the fuselage. A similar mechanism was used to vary the stabilizer pitch angle.

Instrumentation

Electric resistance-wire strain gages were mounted near the root of the stabilizer and fin spars to indicate deflections in bending and torsion. Strain gages were also mounted on the elevator rotation springs to measure elevator angular deflections. Elevator and stabilizer incidence angles were determined by calibrated signals from potentiometers connected to the actuator drive motors. An inclinometer mounted near the model center of gravity measured the fuselage pitch angle.

Comparison of Model and Airplane Properties

In general, the model scaled fairly well the mass properties (table I) and stiffness distributions (fig. 3) of the airplane. In spite of this good agreement in mass and stiffness, the model vibration frequencies (fig. 4) were surprisingly low with frequency ratios (model/airplane) as low as 2.12 compared with the required value of 2.73. However, the

basic character of the individual airplane vibration modes as indicated by the nodal lines appears to be simulated reasonably by the model. One exception was that only one elevator rotation mode of variable phasing (symmetric and antisymmetric) was evident on the model in contrast to one distinct symmetric and antisymmetric mode on the airplane. Since the elevator-rotation and stabilizer-torsion modes were considered most important to the present instability, the ratios of these modes for the original balance weight configuration (fig. 4) were averaged to formulate the final scaling factors which establish the tunnel test conditions. (See the appendix.)

APPARATUS AND TESTS

The investigation was conducted with freon in the Langley transonic dynamics tunnel which has a 16-ft-square (4.88 m) test section (with cropped corners) and is a return-flow, variable-pressure, slotted-throat wind tunnel. It is capable of operation at stagnation pressures from near vacuum to slightly above atmospheric and at Mach numbers from 0 to 1.2. Mach number and dynamic pressure can be varied independently with either air or Freon-12 (dichlorodifluoromethane) used as a test medium. Some physical properties of freon during typical tunnel operation are included in the results table of reference 5. The tunnel is equipped with four quick-opening bypass valves which can be opened to reduce rapidly the dynamic pressure in the test section when flutter occurs.

The model was supported in the tunnel by cables attached to the upper and lower end plates of a four-rod mounting cage which was attached to the model near the center of gravity. Flexure of the four rods permitted model body degrees of freedom in pitch, roll, yaw, and lateral translation (fore-and-aft translation was restricted by drag cables attached near the fuselage nose). A spring located in the vertical support cables permitted model vertical motion. Further details of the model mounting apparatus are described in reference 4.

During the tests, strain-gage signals from the model were continuously recorded on direct readout recorders and magnetic tape. The tunnel test conditions, elevator and stabilizer incidence angles, and fuselage pitch angle were digitized and printed automatically. Visual records of model behavior were provided by high-speed motion pictures.

The test procedure is illustrated by some typical operating paths indicated by the arrows in figure 5. These tunnel paths can be interpreted as the variation in tunnel dynamic pressure $\left(\frac{V}{b(2\pi f_e)\sqrt{\mu}} \approx \sqrt{q}\right)$ with Mach number. For initial tests with the original elevator balance weight configuration, the elevator angle was set at 0^o and the stabilizer angle was adjusted to minimize aerodynamic loads on the various surfaces. At intervals along the operating paths, the tunnel conditions were held constant while the elevators were rotated through an angular range of about $\pm 12^o$ with adjustment in stabilizer pitch

angle to keep the model reasonably trimmed. At several flutter points the stabilizer pitch angle was varied to determine the effect on flutter. After the model conditions for flutter were fairly well established, a slightly different procedure was employed – namely, the flutter condition was approached with the elevator angle set at about $+10^{\circ}$ to $+15^{\circ}$. Basic model frequencies were checked before and after a test of each configuration to insure against visually undetected model damage.

RESULTS AND DISCUSSION

The basic instability phenomenon encountered on the airplane was reproduced by the model in the wind tunnel although the model predicted considerably higher flutter speeds. The fix employed to eliminate the airplane instability was also verified by model tests. The instability exhibited characteristics associated more with flutter than with other dynamic instabilities and will be designated as "flutter" herein. A flutter boundary was traced for the model over the test Mach number range and conditions at which flutter occurred were established. The model test results are compiled in table II and plotted in figure 5. In figure 6, some flutter characteristics of the airplane are compared to those of the model scaled to airplane units by means of the scaling factors presented in the appendix.

Original Elevator Balance Weight Configuration

The model configuration with the original elevator balance weights represented the airplane configuration which fluttered in flight. The model fluttered in a benign, limited-amplitude mode involving a coupled elevator-rotation and stabilizer-torsion motion. The onset of flutter was clearly defined by a small constant amplitude oscillation which did not diverge with increasing time. The model flutter frequency was nearly the same (scaled) frequency as the airplane (fig. 6) and the flutter mode varied randomly from symmetric to antisymmetric motion similarly to that of the airplane. Within the flutter boundary (figs. 5 and 6), flutter began when the elevator was deflected to a positive (trailing-edge-down) angle δ_e of about 8°. Generally, the flutter was preceded by a period of low damped response for approximately 1° of elevator angular travel before becoming sustained. Once the model started fluttering, further increase in δ_e up to a maximum of $+15^{\circ}$ only slightly increased the flutter amplitude. Deflection of the elevator was a necessary requirement for flutter as evidenced by several instances where the flutter boundary was exceeded considerably with $\delta_e \approx 0^{\circ}$ and flutter did not occur until the elevator was deflected to $+8^{\circ}$. It should be noted that no significant variation in model elevator rotation frequency was observed during model vibration tests for elevator deflection angles up to $\pm 12^{\circ}$.

The model did not flutter at negative δ_e up to -15^o (table II) although it was lowly damped at some points, whereas the airplane experienced flutter at elevator angles exceeding 8^o in either direction. The reason for this aspect of the model behavior differing from the airplane is not apparent. One possible explanation is that the damping in the elevator rotation mode may have been somewhat higher for negative elevator angles due to increased bearing friction resulting from tail deflections under static loads. Generally, the static loads were minimized by altering the stabilizer pitch angle for particular elevator angular ranges and the stabilizer was usually close to or within the incidence angle range of the airplane flight flutter points. Varying the stabilizer angle did change the flutter amplitude somewhat but within the limited angular range of the investigation never completely suppressed the flutter. It should be noted that because of the model support freedoms, stabilizer incidence changes were partly negated by a resulting change in fuselage angle of attack; that is, the fuselage pitch angle would vary so as to relieve the loads on the tail imposed by the stabilizer deflections. (The fuselage pitch angle also varied appreciably with elevator deflection.)

The model fluttered at a nearly constant flutter speed index $\frac{V}{b(2\pi f_e)\sqrt{\mu}}$ from a Mach number of about 0.41 to 0.89 (fig. 5). At both extremes of Mach number, the boundary rose sharply and curved inward tending to form a closed region. A possible reason for the boundary upturn at the low Mach numbers is the low mass-density μ range of the model where normally the flutter speed increases rapidly with decreasing μ (ref. 6).

Additional Elevator Balance Weight Configuration

Flutter on the airplane was eliminated within the flight envelope by distributing additional mass balance on the elevator (ref. 1). These added masses increased the elevator static balance from 100 to 142 percent (an elevator nose heavy condition) and the dynamic balance from 54 to 83 percent (established by comparing elevator hinge moments resulting from oscillations in the uncoupled stabilizer torsion mode). With the model representing this airplane configuration, no flutter was obtained up to a flutter speed index which exceeded that for the flutter configuration by about 43 percent at $M = 0.8$. This may also be interpreted as a 43-percent increase in airplane equivalent airspeed.

Comparison of Flutter Characteristics of Model and Airplane

As mentioned previously, horizontal-tail flutter was encountered during airplane flight maneuvers near $M = 0.8$ at altitudes of around 20 000 and 30 000 ft (6096 and 9144 m) (fig. 6) when the elevators were deflected about $\pm 8^o$. Because elevator deflections of this magnitude were not employed in previous flight operations (except possibly during landings), these flutter incidents indicate only that the airplane was within a flutter region enclosing at least the flight flutter points. The model results show (fig. 6) that the

flutter region extends to much lower Mach numbers but predicted considerably higher flutter speeds. The reason for this poor agreement in flutter speed is not known, although some dissimilarities in the model and airplane test conditions existed which could not be readily evaluated. The Reynolds numbers of the airplane flutter points were about 30×10^6 to 45×10^6 with comparable model values ranging from 1.4×10^6 to 4×10^6. Nevertheless, the model was believed sufficiently rough to cause transition fairly far forward on the stabilizer chord at low test Reynolds numbers. Also, at the tunnel test conditions which scaled the airplane flight altitudes (established from the relationship $\left[\frac{V}{b(2\pi f_i)\sqrt{\mu}}\right]_{model} = \left[\frac{V}{b(2\pi f_i)\sqrt{\mu}}\right]_{airplane}$), the model individual values of μ and $\frac{V}{b(2\pi f_i)}$ were about 3.2 and 1.8 times greater, respectively, than the corresponding values for the airplane. (See the appendix.)

Originally, the airplane flutter was thought to involve shock-induced separated flow resulting from the elevator deflection. Since the model fluttered at Mach numbers as low as 0.41, shocks would not be expected to form at these low Mach numbers even at the maximum elevator angles investigated ($\pm 15^o$). However, the flow over or near the elevator could separate due simply to elevator deflections of the magnitude at which flutter began ($\approx 8^o$). A clue to a possible flutter mechanism is suggested by the analytical results (ref. 1) wherein a solution was forced at an airplane flutter condition by reducing the elevator aerodynamic hinge moment to about one-half the nominal incompressible flow value. Physically, a comparable result could be obtained by flow separation over the elevator which reduces the aerodynamic loads on the elevator and, more importantly, changes the relative aerodynamic loads between the elevator and stabilizer. Thus, the flutter mechanism probably involves a dynamic coupling of the elevator-rotation and stabilizer-torsion modes resulting from the aerodynamic forces associated with separated flow over or near the elevator. In any event, the additional elevator balance weights apparently decoupled the elevator-rotation and stabilizer-torsion modes sufficiently to preclude flutter at the airplane flight test points and within the model test limits.

CONCLUSIONS

An exploratory study of a deflected-elevator flutter encountered on a large T-tail airplane has been conducted with a 1/8.5-size empennage flutter model in the Langley transonic dynamics tunnel at Mach numbers up to 0.93. The following results were obtained:

1. The basic flutter phenomenon experienced by the airplane was reproduced by the model in the wind tunnel although the model predicted considerably higher flutter speeds.

2. The model required an elevator angle of $+8^{\circ}$ (trailing-edge-down) to initiate flutter, whereas the airplane fluttered at elevator angles of 8° in either up or down direction. Variations in model stabilizer incidence angle did affect the flutter amplitude somewhat but within the limited stabilizer incidence angles of the present tests did not completely suppress the flutter.

3. The model fluttered at roughly the same equivalent airspeed from a Mach number of about 0.41 to 0.89. At the extreme Mach numbers, the flutter speed boundary rose sharply and curved inward tending to form a closed region.

4. Elevator mass balancing, used to eliminate flutter on the airplane, also eliminated flutter on the model.

Langley Research Center,
National Aeronautics and Space Administration,
Langley Station, Hampton, Va., October 31, 1968,
737-02-00-01-23.

APPENDIX

MODEL SCALING

The present study employed an existing flutter model of an early horizontal-tail design which was scaled to satisfy the following requirements:

(1) $\left[\text{Mach number}\right]_{\text{model}} = \left[\text{Mach number}\right]_{\text{airplane}}$

(2) $\mu_{\text{model}} = \mu_{\text{airplane}}$

(3) $$\left[\frac{V}{b(2\pi f_i)}\right]_{\text{model}} = \left[\frac{V}{b(2\pi f_i)}\right]_{\text{airplane}}$$

In modifying the model to conform to current airplane values, it was necessary to compromise requirements (2) and (3). Consequently, the model test conditions were related to airplane flight conditions so that

(4) $$\left[\frac{V}{b(2\pi f_i)\sqrt{\mu}}\right]_{\text{model}} = \left[\frac{V}{b(2\pi f_i)\sqrt{\mu}}\right]_{\text{airplane}}$$

Squaring both sides and expanding μ yield the following relationship:

$$\left[\frac{\rho V^2}{b^2(2\pi f_i)^2 \frac{m_h}{V}}\right]_{\text{model}} = \left[\frac{\rho V^2}{b^2(2\pi f_i)^2 \frac{m_h}{V}}\right]_{\text{airplane}}$$

hence,

$$q_R = \frac{m_R f_R^2}{l_R}$$

These and other important scaling ratios are presented in the following table. Following usual practice, the final tunnel test conditions were established by using measured scaling factors. It should be noted that at a model test condition which simulated a particular airplane flight altitude, although requirement (4) was satisfied, the individual values of μ and $\frac{V}{b(2\pi f_i)}$ for the model were considerably different from those for the airplane.

APPENDIX

Quantity	Scaling ratio, Model/Airplane		
	Symbol	Required	Final adjusted
Mach number		1.0	1.0
$V/b(2\pi f_i)\sqrt{\mu}$		1.0	1.0
μ		2.40	[a]3.19
$V/b(2\pi f_i)$		1.55	[a]1.79
Length	l_R	1/8.465	[a]1/8.465
Mass	m_R	1/404	[a]1/404
EI and GJ		1/32862	[a]1/32862
Natural vibration frequency (f_i)	f_R	2.73	[a]2.37
Stream velocity (V)		1/2.00	1/2.00
Stream dynamic pressure (q)	q_R	1/6.40	1/8.50
Stream density (ρ)		1/1.60	1/2.12

To convert tunnel test conditions to airplane equivalent airspeed:

$$V_{KEAS}\ (\text{Knots}) = 17.186\sqrt{q(\text{psf})}$$

$$q_{airplane} = q_{model} \times \frac{1}{q_R} = q_{model} \times 8.50$$

$$V_{KEAS,airplane} = 50.1\sqrt{q_{model}(\text{psf})}$$

[a]Most representative value. Frequency scaling factor is average factor for natural vibration modes considered most important in present flutter. (See footnote a in fig. 4.)

REFERENCES

1. McAvoy, J. M.: C-141A Empennage Flutter Substantiation With Revised Elevator Balance Weights. Rep. No. ER-8471, Lockheed-Georgia Co., June 15, 1966.

2. Jones, W. P., ed.: Manual on Aeroelasticity. Volume V – Factual Information on Flutter Characteristics. AGARD.

3. Bisplinghoff, Raymond L.; Ashley, Holt; and Halfman, Robert L.: Aeroelasticity. Addison-Wesley Pub. Co., Inc., c.1955.

4. Sandford, Maynard C.; Ruhlin, Charles L.; and Yates, E. Carson, Jr.: Subsonic and Transonic Flutter and Flow Investigations of the T-Tail of a Large Multijet Cargo Airplane. NASA TN D-4316, 1968.

5. Ruhlin, Charles L.; Sandford, Maynard C,; and Yates, E. Carson, Jr.: Wind-Tunnel Flutter Studies of the Sweptback T-Tail of a Large Multijet Cargo Airplane at Mach Numbers up to 0.90. NASA TN D-2179, 1964.

6. Yates, E. Carson, Jr.; Land, Norman S.; and Foughner, Jerome T., Jr.: Measured and Calculated Subsonic and Transonic Flutter Characteristics of a 45^{o} Sweptback Wing Planform in Air and in Freon-12 in the Langley Transonic Dynamics Tunnel. NASA TN D-1616, 1963.

TABLE I.- MASS PROPERTIES OF MODEL CONFIGURATIONS

Total model:		
Mass, slugs (kg)	7.23	(105.51)
Center of gravity, in. (cm)	FS 101.90	(258.8)
Fuselage mass, slugs (kg)	3.44	(50.20)
Wing and pylon-nacelle:		
Wing mass (full-span), slugs (kg)	1.878	(27.407)
Pylon-nacelle mass (both sides), slugs (kg)	1.467	(21.409)
Inertia in roll about fuselage center line, slug-ft^2 (kg-m^2)	36.261	(49.16)
Vertical tail mass, slugs (kg)	0.172	(2.51)
Horizontal tail (original balance weights)[a]:		
Mass, slugs (kg)	0.2687	(3.92)
m_h (semispan), slugs (kg)	0.1000	(1.46)
Center of gravity, in. (cm)	FS 205.0	(520.7)
I_θ, slug-ft^2 (kg-m^2)	0.0729	(0.0988)
I_ψ, slug-ft^2 (kg-m^2)	0.556	(0.754)
I_ϕ, slug-ft^2 (kg-m^2)	0.506	(0.686)
Horizontal tail (additional balance weights)[a]:		
Mass, slugs (kg)	0.2865	(4.181)
m_h (semispan), slugs (kg)	0.1089	(1.589)
Center of gravity, in. (cm)	FS 205.4	(521.7)
I_θ, slug-ft^2 (kg-m^2)	0.0827	(0.112)
I_ψ, slug-ft^2 (kg-m^2)	0.6286	(0.852)
I_ϕ, slug-ft^2 (kg-m^2)	0.5710	(0.774)

[a]Includes stabilizer, elevators, and components enclosed in bullet fairing. Exception is m_h which is semispan value.

Typical stabilizer without elevator

Section	Section limits, η_{ea}	Mass		S_{ea}		I_{ea}	
		slugs	kg	slug-ft	kg-m	slug-ft^2	kg-m^2
1	0.0633 to 0.2208	0.0197	0.289	-0.323×10^{-3}	-0.00144	2.040×10^{-3}	0.00277
2	.2208 to .3727	.0150	.220	+.178	+.00079	1.300	.00176
3	.3727 to .5234	.0105	.153	-.276	-.00123	.621	.00084
4	.5234 to .6719	.0103	.150	-.200	-.00089	.506	.00069
5	.6719 to .8255	.0076	.111	-.248	-.00110	.269	.00036
6	.8255 to 1.0000	.0072	.106	+.059	+.00026	.171	.00023
Total	0.0633 to 1.0000	0.0703	1.029	-0.810×10^{-3}	-0.00361	4.907×10^{-3}	0.00665

Typical elevator

Configuration	Mass balance, percent	Mass		$S_{h\ell}$		$I_{h\ell}$	
		slugs	kg	slug-ft	kg-m	slug-ft^2	kg-m^2
Original balance weights	100	0.0297	0.434	$+0.0233 \times 10^{-3}$	+0.000103	0.220×10^{-3}	0.000298
Additional balance weights	142	.0386	.564	-.2730	-.00121	.236	.000319

Components enclosed in bullet fairing

Component	Mass		Center of gravity		I_θ		I_ψ		I_ϕ	
	slugs	kg	in.	cm	slug-ft^2	kg-m^2	slug-ft^2	kg-m^2	slug-ft^2	kg-m^2
Bullet fairing	0.0223	0.326	FS 201.2	FS 511.0	0.0123	0.01668	$\approx I_\theta$		-------	-------
Elevator actuator mechanism	.0290	.423	FS 202.7	FS 514.8	.00152	.00206	0.001606	0.00218	0.000727	0.000984
Stabilizer spar center section	.0174	.254	FS 198.1	FS 503.2	.00299	.00405	$\approx I_\theta$		-------	-------

TABLE II.- SUMMARY OF TEST RESULTS

Model behavior (a)	M	q		V		ρ		R	f, cps	μ	$\frac{V}{b(2\pi f_e)\sqrt{\mu}}$	Flutter δ_e, deg	No flutter δ_e, deg	δ_s, deg (b)	α_s, deg (b)
		lb/ft^2	kN/m^2	μ/sec	m/s	$slug/ft^3$	kg/m^3								
Original elevator balance weight configuration															
NF	0.817	15.1	0.72	413.3	126.0	0.000177	0.091	0.33×10^6	---	198.9	0.1588	-----	-14 to +16	2.5 to 0.2	6.2 to 1.4
NF	.919	18.3	.88	462.8	141.1	.000171	.088	.365	---	205.8	.1748	-----	-14 to +16	2.9 to .2	5.4 to 2.3
NF	.929	48.0	2.30	478.7	145.9	.000418	.215	.89	---	84.2	.2827	-----	-13 to +15	2.0 to .1	4.6 to 3.2
NF	.928	82.7	3.96	466.3	142.1	.000759	.391	1.63	---	46.4	.3710	-----	-11 to +15	1.9 to .1	4.7 to 4.5
NF	.379	67.8	3.25	191.5	58.4	.003662	1.887	3.19	---	9.6	.3350	-----	+10.6	.2	2.2
F	.459	96.9	4.64	231.3	70.5	.003589	1.850	3.77	53.1	9.8	.4006	≧10.7	---------	.2	2.8
F	.414	58.3	2.79	209.1	63.7	.002647	1.364	2.52	53.3	13.3	.3107	≧7.5	---------	.2	2.6
F	.496	51.6	2.47	250.6	76.4	.001635	.843	1.86	53.7	21.5	.2929	≧8.9	---------	.1	2.4
F	.563	49.0	2.35	286.4	87.3	.001191	.614	1.53	53.3	29.6	.2853	≧9.0	-14 to +9	2.0 to .2	6.2 to 2.3
F	.622	51.6	2.47	316.7	96.5	.001026	.529	1.46	52.9	34.3	.2930	≧9.9	---------	.2	3.2
F	.734	54.1	2.59	373.7	113.9	.000773	.398	1.30	53.6	45.5	.3002	≧9.7	-12 to +10	2.0 to .1	6.0 to 2.9
F	.832	62.1	2.97	420.3	128.1	.000701	.361	1.34	53.8	50.2	.3215	≧7.8	-12 to +8	2.9 to -1.5	6.9 to 3.5
F	.885	67.7	3.24	445.7	135.8	.000680	.350	1.39	54.1	51.8	.3355	≧7.8	-11 to +8	2.0 to .2	5.3 to 4.0
F	.852	73.9	3.54	429.5	130.9	.000799	.412	1.57	53.6	44.0	.3510	≧8.0	-11 to +8	2.1 to .1	5.5 to 4.6
F	.849	84.3	4.04	428.0	130.4	.000917	.473	1.79	54.3	38.4	.3744	≧9.9	---------	0	4.8
Additional elevator balance weight configuration															
NF	0.723	20.8	1.00	365.7	111.5	0.000310	0.160	0.51×10^6	---	124.2	0.1804	-----	-11 to +15	2.0 to 0.2	6.3 to 2.8
NF	.822	25.3	1.21	413.6	126.1	.000295	.152	.56	---	130.5	.1991	-----	-12 to +15	2.0 to .2	6.7 to 3.2
NF	.917	29.6	1.42	459.7	140.1	.000279	.144	.60	---	138.0	.2151	-----	-11 to +15	2.0 to .1	5.5 to 4.0
NF	.726	44.0	2.11	368.6	112.3	.000645	.332	1.07	---	59.7	.2622	-----	-11 to +15	2.0 to .1	6.5 to 2.9
NF	.834	53.8	2.58	420.9	128.3	.000606	.312	1.17	---	63.5	.2904	-----	-11 to +14	2.1 to .1	6.1 to 4.0
NF	.910	61.0	2.92	458.3	139.7	.000579	.298	1.22	---	66.5	.3089	-----	-11 to +15	2.0 to .1	5.1 to 4.4
NF	.716	71.0	3.40	363.9	110.9	.001068	.550	1.75	---	36.0	.3333	-----	-11 to +10	2.1 to .1	6.1 to 4.2
NF	.861	94.0	4.50	435.2	132.6	.000989	.510	1.96	---	38.9	.3835	-----	-11 to +11	2.1 to .1	5.6 to 4.9
NF	.543	44.6	2.14	277.7	84.6	.001152	.594	1.44	---	33.4	.2640	-----	+11	.1	3.1
NF	.536	66.0	3.16	271.0	82.6	.001788	.921	2.20	---	21.5	.3213	-----	-10 to +11	2.0 to .1	6.2 to 3.6
NF	.697	103.5	4.96	351.1	107.0	.001671	.861	2.69	---	23.0	.4024	-----	-10 to +11	2.0 to .1	5.5 to 4.7
NF	.811	131.2	6.28	407.2	124.1	.001575	.812	2.94	---	24.4	.4531	-----	-10 to +11	2.0 to .1	5.2
NF	.435	45.5	2.18	221.9	67.6	.001838	.947	1.84	---	20.9	.2669	-----	-10 to +11	2.0 to .1	6.5 to 3.0

[a]Model behavior code:

NF No flutter within δ_e range indicated.

F Flutter at δ_e or greater positive angles. No flutter in δ_e range indicated.

[b]The values of δ_s and α_s in these angular ranges are generally related by the listed order to a δ_e value and to each other. For example, in the first line of data at $\delta_e = -14^o$, $\delta_s = 2.5^o$, and $\alpha_s = 6.2^o$.

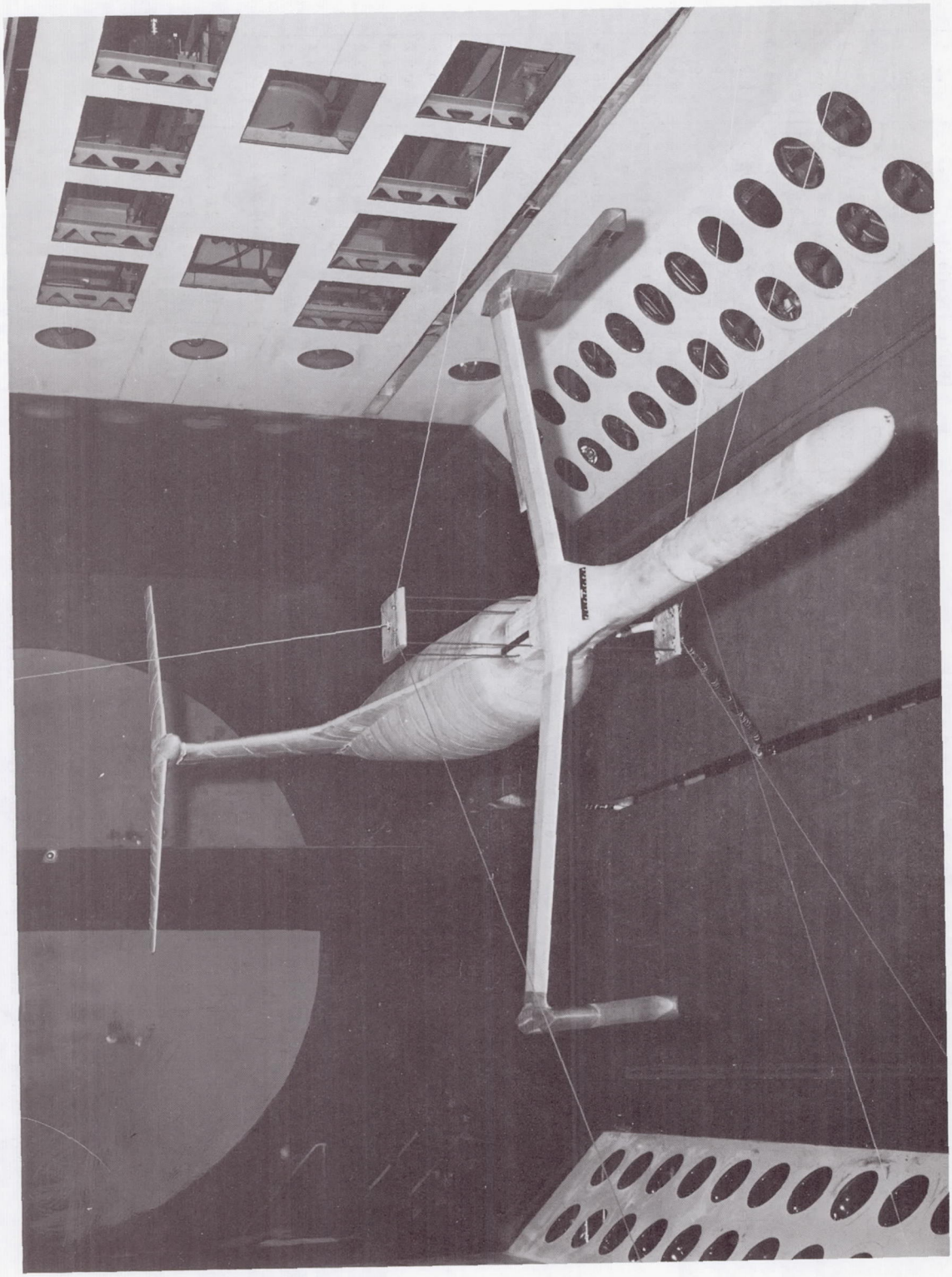

L-62-6734

Figure 1.- Photograph of complete model in tunnel.

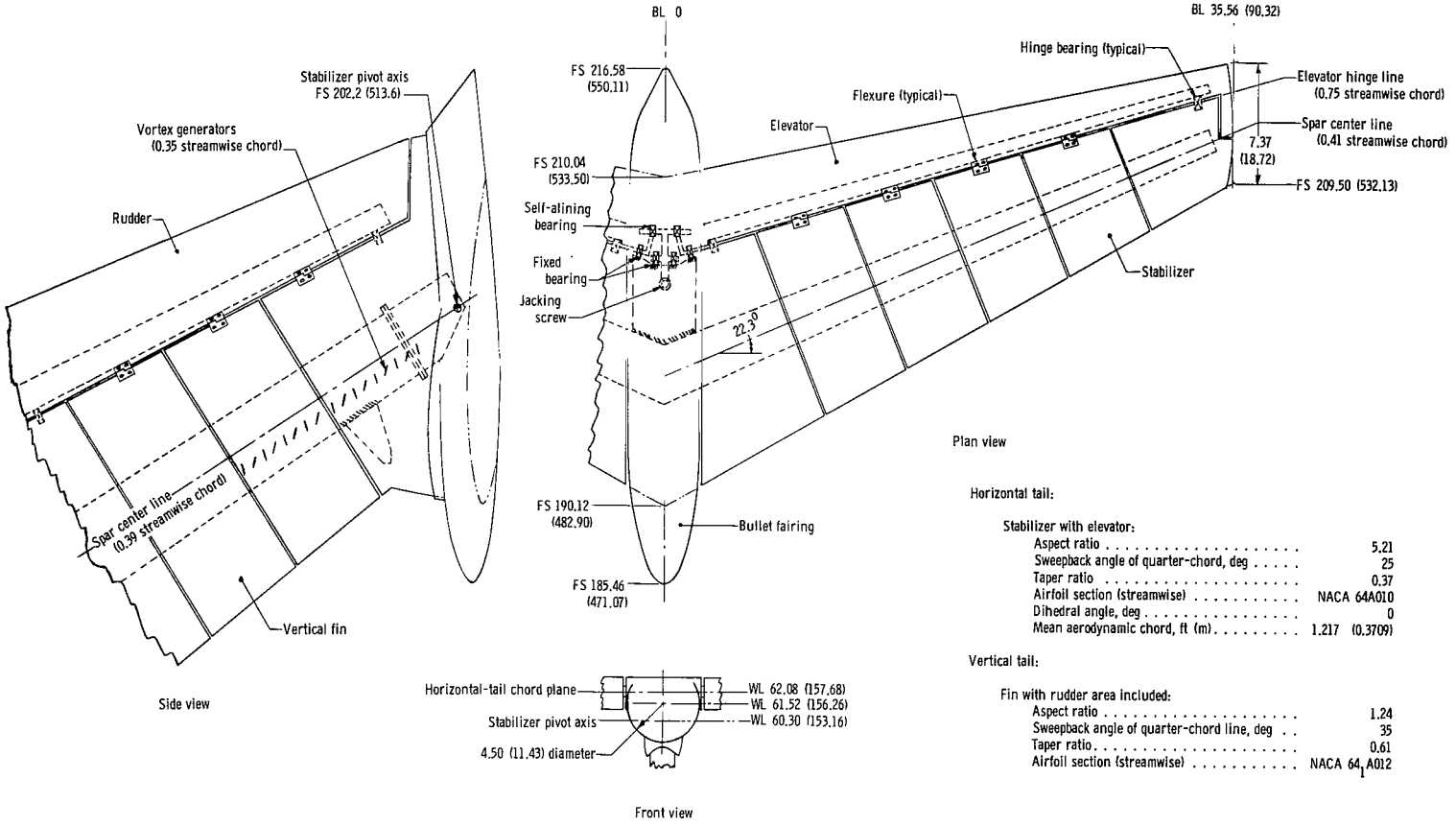

Horizontal tail:

Stabilizer with elevator:

Aspect ratio	5.21
Sweepback angle of quarter-chord, deg	25
Taper ratio	0.37
Airfoil section (streamwise)	NACA 64A010
Dihedral angle, deg	0
Mean aerodynamic chord, ft (m)	1.217 (0.3709)

Vertical tail:

Fin with rudder area included:

Aspect ratio	1.24
Sweepback angle of quarter-chord line, deg	35
Taper ratio	0.61
Airfoil section (streamwise)	NACA 64_1A012

Figure 2.- Sketches of model. All dimensions are in in. (cm) except as noted otherwise.

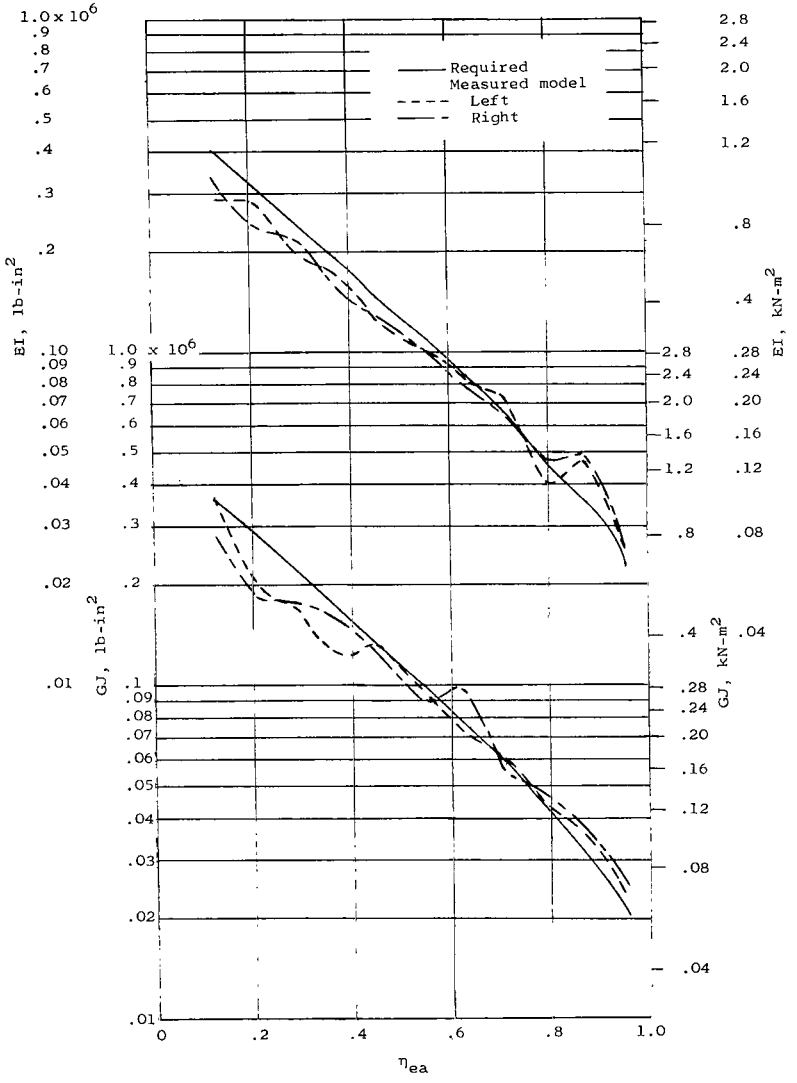

(a) Stabilizer spars.

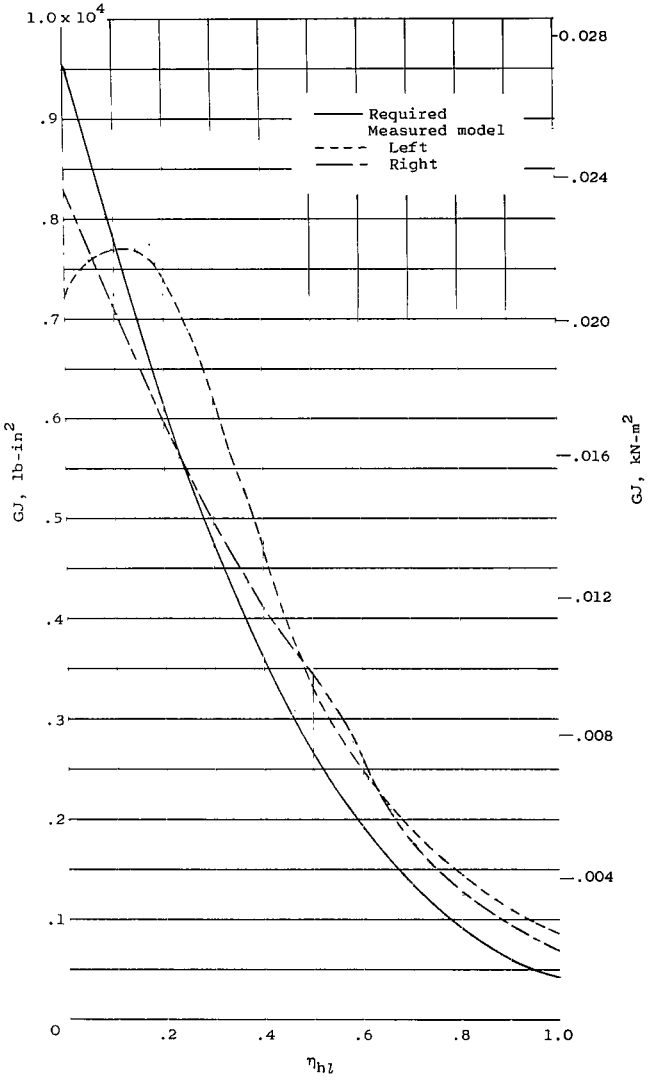

(b) Elevators.

Figure 3.- Measured distribution of bending and torsional stiffnesses of stabilizer spars and elevators.

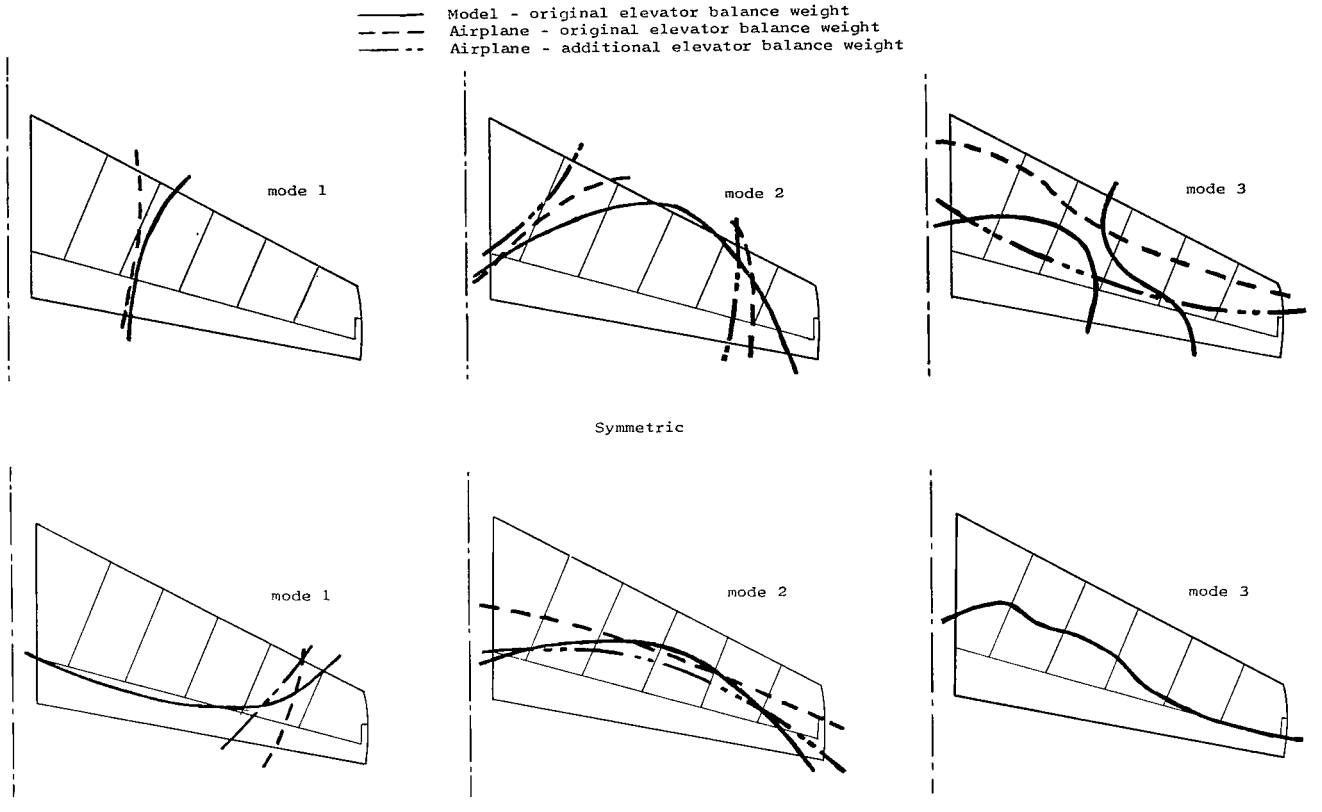

Vibration Mode	Original elevator balance weight			Additional elevator balance weight		
	Measured frequency, cps		Ratio	Measured frequency, cps		Ratio
	Model	Airplane	Model/Airplane	Model	Airplane	Model/Airplane
			Symmetric			
mode 1 - stabilizer first bending	16.2	6.29	2.57	not measured	not measured	-
mode 2 - stabilizer second bending	56.0	21.9	2.56	not measured	21.2	-
mode 3 - stabilizer torsion	78.0	28.5	[a]2.74	not measured	27.7	-
elevator rotation [b]	[c]35.4	15.7	[a]2.25	34.9	15.1	2.31
			Antisymmetric			
mode 1 - stabilizer bending	43.6	17.0	2.56	not measured	16.6	-
mode 2 - stabilizer torsion	61.4	29.0	[a]2.12	[d]60.0	26.7	2.25
mode 3 - unidentified	78.8	not measured	-	not measured	not measured	-
elevator rotation [b]	[c]35.4	not measured	-	34.9	14.4	2.42
Flutter (phasing varies)	[c]53.6	[c]24.0	2.23	no flutter		

[a]These three frequency ratios were averaged to obtain a frequency ratio of 2.37 for scaling purposes.
[b]Node lines were coincident with elevator hinge line.
[c]Average of measured frequencies - exhibited both symmetric and antisymmetric phasing. The model elevator rotation frequency did not vary significantly with elevator deflection angles up to $\pm$ 12°.
[d]Node line was same as the original elevator balance weight configuration.

Figure 4.- Measured node lines and natural vibration frequencies for model and airplane configurations.

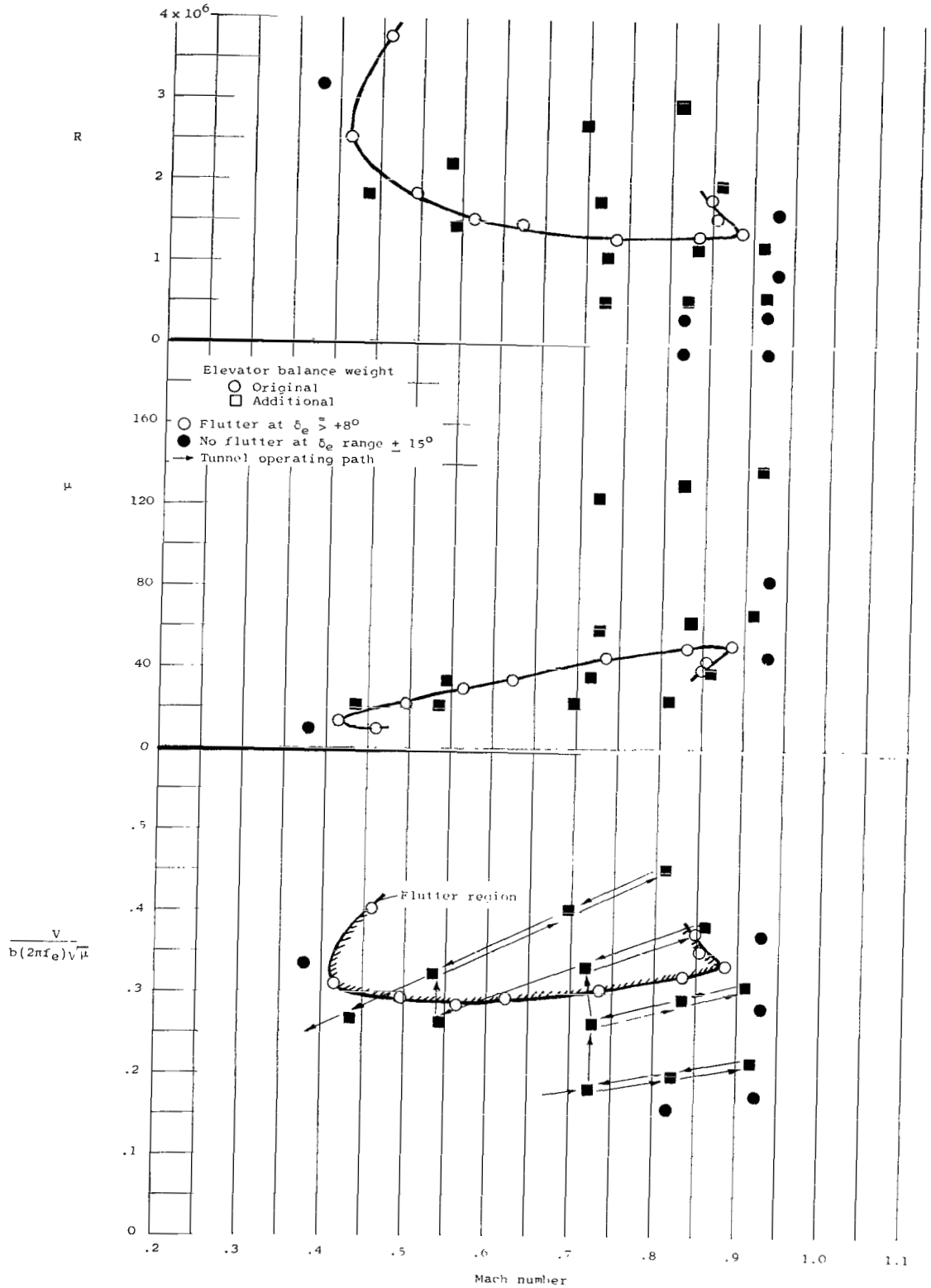

Figure 5.- Experimental results for model with different elevator balance weights.

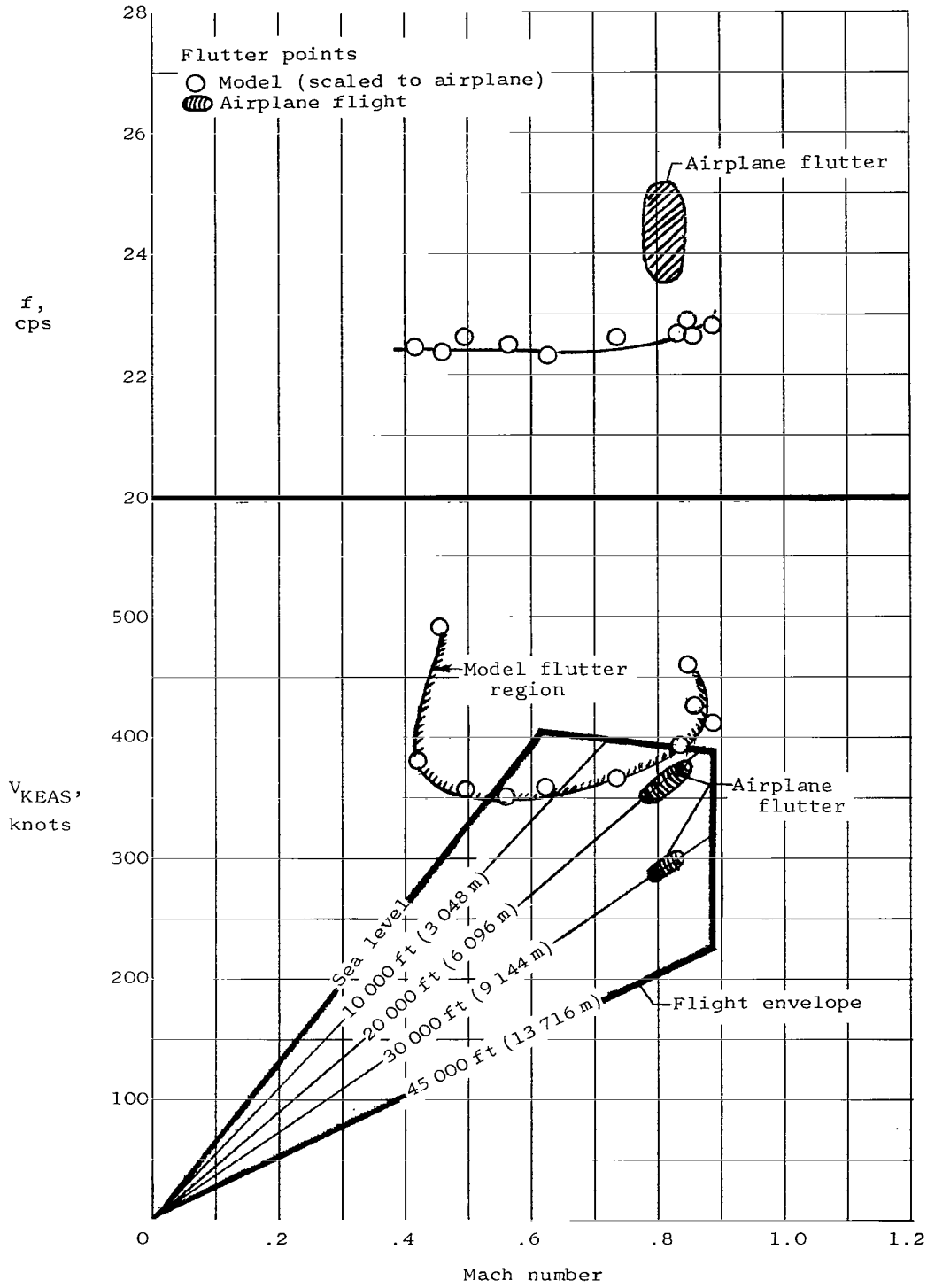

Figure 6.- Comparison between model and airplane flutter characteristics. Units are full-scale airplane values.